nanomaterials

MDPI

Article

Strong Tribocatalytic Nitrogen Fixation of Graphite Carbon Nitride g-C_3N_4 through Harvesting Friction Energy

Zheng Wu [1,*], Taosheng Xu [1], Lujie Ruan [2], Jingfei Guan [2,*], Shihua Huang [2], Xiaoping Dong [3], Huamei Li [2] and Yanmin Jia [4,*]

[1] Xi'an Key Laboratory of Textile Chemical Engineering Auxiliaries, School of Environmental and Chemical Engineering, Xi'an Polytechnic University, Xi'an 710048, China; xutaosheng2021@126.com
[2] College of Physics and Electronic Information Engineering, Zhejiang Normal University, Jinhua 321004, China; lujie_ruan@foxmail.com (L.R.); huangshihua@zjnu.cn (S.H.); lihuamei@zjnu.cn (H.L.)
[3] Key Laboratory of Surface & Interface Science of Polymer Materials of Zhejiang Province, Department of Chemistry, Zhejiang Sci-Tech University, Hangzhou 310018, China; xpdong@zstu.edu.cn
[4] School of Science, Xi'an University of Posts and Telecommunications, Xi'an 710121, China
* Correspondence: wuzheng@xpu.edu.cn (Z.W.); jingfei_guan@foxmail.com (J.G.); jiayanmin@xupt.edu.cn (Y.J.)

Abstract: Mechanical energy derived from friction is a kind of clean energy which is ubiquitous in nature. In this research, two-dimensional graphite carbon nitride (g-C_3N_4) is successfully applied to the conversion of nitrogen (N_2) fixation through collecting the mechanical energy generated from the friction between a g-C_3N_4 catalyst and a stirring rod. At the stirring speed of 1000 r/min, the tribocatalytic ammonia radical (NH_4^+) generation rate of g-C_3N_4 can achieve 100.56 μmol·L^{-1}·g^{-1}·h^{-1} using methanol as a positive charge scavenger, which is 3.91 times higher than that without any scavengers. Meanwhile, ammonia is not generated without a catalyst or contact between the g-C_3N_4 catalyst and the stirring rod. The tribocatalytic effect originates from the friction between the g-C_3N_4 catalyst and the stirring rod which results in the charges transfer crossing the contact interface, then the positive and negative charges remain on the catalyst and the stirring rod respectively, which can further react with the substance dissolved in the reaction solution to achieve the conversion of N_2 to ammonia. The effects of number and stirring speed of the rods on the performance of g-C_3N_4 tribocatalytic N_2 fixation are further investigated. This excellent and efficient tribocatalysis can provide a potential avenue towards harvesting the mechanical energy in a natural environment.

Keywords: tribocatalysis; g-C_3N_4; N_2 fixation; ammonia generation; friction

Citation: Wu, Z.; Xu, T.; Ruan, L.; Guan, J.; Huang, S.; Dong, X.; Li, H.; Jia, Y. Strong Tribocatalytic Nitrogen Fixation of Graphite Carbon Nitride g-C_3N_4 through Harvesting Friction Energy. *Nanomaterials* **2022**, *12*, 1981. https://doi.org/10.3390/nano12121981

Academic Editor: Gianvito Vilé

Received: 27 April 2022
Accepted: 8 June 2022
Published: 9 June 2022

1. Introduction

Nowadays, due to the immoderate consumption and mining of fossil fuels, energy shortage and environment pollution have become critical issues which are a threat to the survival and development of society [1]. Accordingly, it is necessary to look for renewable and green energy to replace these fossil fuels. Ammonia has been regarded as a green energy source with some advantages such as no carbon dioxide emission, high energy density and convenient transportation [2,3]. Nevertheless, how to perform ammonia production is also a vital issue. At present, various methods have been reported to convert nitrogen (N_2) to ammonia (NH_3), such as thermocatalytic reduction, electrocatalytic reduction and photocatalytic reduction [4–6]. However, thermocatalytic and electrocatalytic reduction usually require high-pressure or high-temperature operating conditions, which limit the actual application of ammonia production [7,8]. Additionally, photocatalytic reduction of nitrogen can be performed at a mild condition, but low light utilization efficiency would seriously hinder the actual production of ammonia [9]. Therefore, it is crucial to seek mild and highly efficient approaches for nitrogen reduction.

In nature, mechanical energy is widespread distributed energy, which exists in wind, river flows and human movement [10]. If such abundant energy can be successfully har-

vested for the reduction of nitrogen, it would be meaningful to propel the production of ammonia. Tribocatalysis, which can convert the friction of mechanical energy into the electric energy via persistent friction, has attracted the attention of researchers [11–13]. Under friction, when two different kinds of materials contact each other, chemical bonds will form through physical contact on the interface [14]. After being separated, two materials will carry the positive or negative charges respectively, due to breakage of the chemical bonds [15]. Then the free charges generated via the triboelectric process can be further applied to the catalytic reaction such as dye degradation, carbon dioxide or flammable gas production [16–20]. However, to date, there has been no report about harvesting the mechanical energy from friction via tribocatalysis for nitrogen reduction to produce ammonia.

Graphite carbon nitride (g-C_3N_4) is an emerging semiconductor material with layered structure similar to graphite [21]. The C and N atoms inside it are arranged alternately through sp^2 hybridization [22]. g-C_3N_4 is a candidate catalyst in several catalytic areas such as the decomposition of organic pollutants [23–25], hydrogen evolution [26,27] and carbon dioxide reduction [28–30] based on its advantages of being insoluble in water and having a large specific surface area and stable chemical properties. In 2019, Xia et al. achieved the photocatalytic synthesis of ammonia from nitrogen through using a defecting g-C_3N_4 catalyst. After 100 min light irradiation, the yield of ammonia can be up to 54 μmol/L [31]. Dong et al. achieved highly efficient dichlorophenols decomposition via photocatalysis using g-C_3N_4 [23]. Recent studies have found that mesoporous carbon nitride materials can exhibit excellent catalytic activity through introducing metal atoms inside them. Gianvito Vilé et al. have reported that Cu-based single-atom catalysts developed on a mesoporous carbon nitride carrier exhibited excellent catalytic activity during the synthesis of triazoles [32]. Liu et al. found that the photocatalytic decomposition activity of gemfibrozil can be significantly improved by introducing Ag or Cu atoms into the mesoporous carbon nitride skeleton, which is related to ligand-to-metal charge transfer (LMCT) or ligand-to-metal-to-ligand charge transfer (LMLCT) [33]. Based on the above analysis, g-C_3N_4 is hopeful for applications in highly efficient tribocatalytic nitrogen fixation, which is not reported at present.

In this work, the excellent tribocatalytic reduction of nitrogen to ammonia under stirring is achieved in g-C_3N_4 which is fabricated via the chemical blowing method. After 10 h stirring at room temperature in the dark, the tribocatalytic ammonia radical (NH_4^+) generation rate is up to about 100.56 $\mu mol \cdot L^{-1} \cdot g^{-1} \cdot h^{-1}$ using a positive charge scavenger (methanol), which is 3.91 times higher than that without any charge scavengers. In addition, the effects of a negative charge scavenger, the number and speed of stirring rods, and the contact area between the catalyst and stirring rods in tribocatalysis on the performance of g-C_3N_4 tribocatalytic N_2 fixation are also investigated. The possible tribocatalytic mechanism of N_2 fixation has been also proposed. As the N_2 fixation research continues to thrive and expand, the finding in this work provides a great potential application to harvest the mechanical energy via tribocatalysis for clean energy production.

2. Materials and Methods

2.1. Preparation of g-C_3N_4 Sample

g-C_3N_4 used in this research was prepared according to the reported chemical blowing method [34,35]. A certain amount of ammonium chloride (16 g) and melamine (4 g) were accurately weighed and then mixed together. The mixture was thoroughly ground in a mortar and placed in a crucible. Then, it was stuffed into the muffle furnace, heated from room temperature to 550 °C (6 °C/min), and the calcination time was set to 4 h. After the calcination, the faint yellow product in the crucible was collected and ground through an agate mortar to obtain g-C_3N_4.

2.2. Characterization

The X-ray diffraction pattern of the g-C_3N_4 sample was tested on a D8 Advance diffractometer (Bruker AXS, Karlsruhe, Germany). The micro morphology of the sample was examined with a scanning electron microscope (Gemini SEM 300, ZEISS, Oberkochen, Germany). The chemical properties of the sample were analyzed through using the X-ray photoelectron spectrometer (XPS, ESCALAB 250Xi, Waltham, MA, USA). The infrared spectra of the sample prepared through the KBr tablet pressing method were characterized via the Fourier transform infrared spectrometer (FTIR, Nicolet NEXUS 670, Ramsey, MN, USA). The content of ammonia (NH_4^+) was analyzed via a UV-Vis spectrophotometer (Ocean Optics QE65Pro, Dunedin, FL, USA).

2.3. Tribocatalytic Performance Measurements

To investigate g-C_3N_4 tribocatalytic performance, N_2 fixation experiments were performed. A total of 50 mL methanol solution (containing 5 mL methanol and 45 mL DI water) mixed with 50 mg g-C_3N_4 was contained in a brown bottle. The solution was then placed under shading conditions and stirred at 1000 rpm for 2 h through a polytetrafluoroethylene (PTFE) stirring rod with a specification of $\varnothing$ 6 $\times$ 20 mm^2 to achieve adsorption-desorption equilibrium. Then under continuous stirring, the suspension of 3 mL was collected through a rubber-tipped dropper every 2 h of stirring. The supernatan was obtained through a centrifuge (3 min, 6500 rpm). The generation of NH_4^+ produced in the process of tribocatalysis was determined through the colorimetric method, and Nessler reagent was selected as the indicator [36,37]. Then 40 μL sodium tartrate solution (0.5 $g{\cdot}mL^{-1}$) and 60 μL Nessler's reagent were added dropwise into supernatant and left to stand for 12 min to react sufficiently. Finally, the content of ammonium was analyzed at the peak of ~420 nm via a UV–Vis spectrophotometer.

3. Results and Discussion

SEM images of the g-C_3N_4 sample before the tribocatalytic N_2 fixation reaction are depicted in Figure 1. g-C_3N_4 samples show the agglomerate morphology composed of many irregular ultra-thin two-dimensional sheet-like structures. From Figure 1, g-C_3N_4 catalyst material composed of many huge flakes has a large specific surface area.

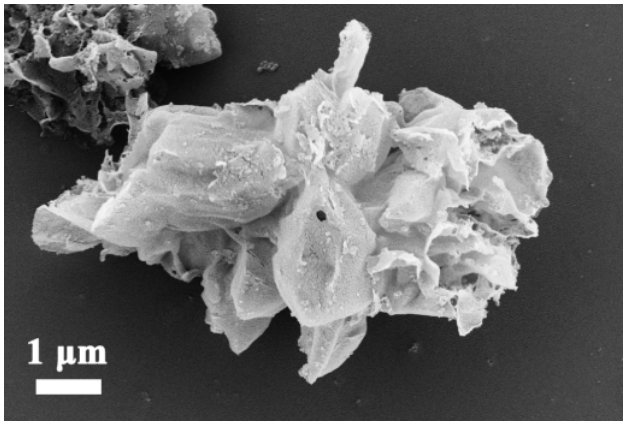

Figure 1. SEM image of g-C_3N_4.

The crystal diffraction patterns of g-C_3N_4 have been measured with XRD, as shown in Figure 2. The obvious peaks at 2θ value of 12.93° and 27.69° are corresponding to the (100) and (002) crystal plane of g-C_3N_4 through referring the standard card PDF#87-1526. It is ascribed to the orderly stacking of the conjugated carbon-nitrogen heterocycles in a planar and layered framework, respectively [38,39]. In addition, the high-intensity diffraction peaks and the absence of other impurity peaks indict the excellent synthesis of g-C_3N_4.

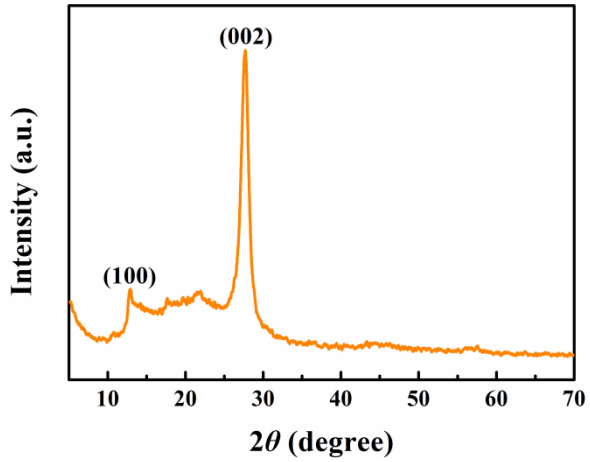

Figure 2. XRD patterns of g-C_3N_4.

FTIR spectra depicted in Figure 3 reveal the functional groups of g-C_3N_4 before the tribocatalytic N_2 fixation. The peak around the wave number of 812 cm^{-1} is caused by the out-of-plane bending vibration of the triazine structure [40,41]. The peaks in the wave number range of 1240–1640 cm^{-1} are related to the stretching vibration mode of C–N heterocycle in the g-C_3N_4 sample [23]. The broad peaks in the range of 3080–3450 cm^{-1} are ascribed to the stretching vibrations of N−H and O−H groups [39,42].

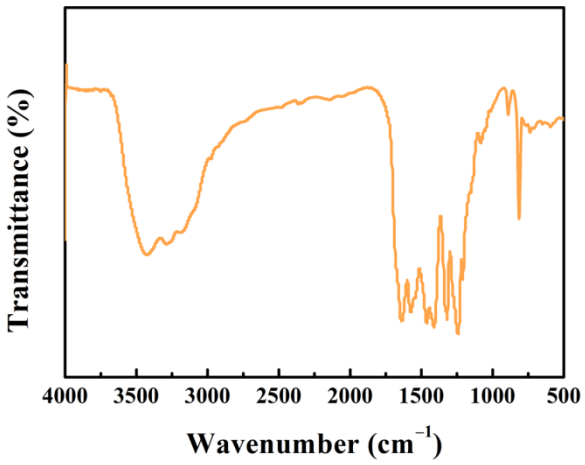

Figure 3. FTIR spectra of g-C_3N_4.

The elemental states of the g-C_3N_4 sample have been performed with XPS measurement, as depicted in Figure 4. From Figure 4a, the measured survey spectrum confirms the inclusion of both C and N elements in g-C_3N_4. The high-resolution XPS spectrum of C 1s are presented in Figure 4b. The spectrum of C 1s has two peaks at 284.42 eV and 287.22 eV, which are assign to graphitic carbon adsorbed on the sample surface and sp^2-bonded carbon in the triazine structure [39]. As shown in Figure 4c, the N 1s spectrum of g-C_3N_4 was deconvoluted into three peaks at binding energies of 397.72 eV, 398.87 eV and 400.07 eV, corresponding to C=N−C, N−$(C)_3$ and N−H in the sample, respectively [38,43].

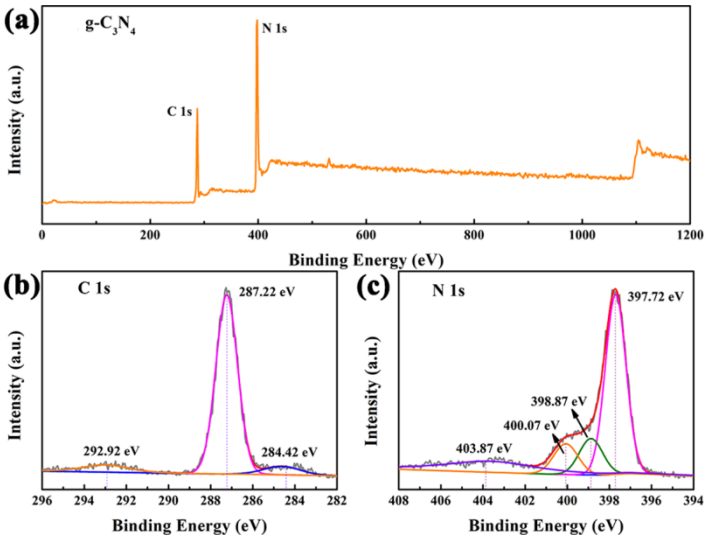

Figure 4. XPS spectra of g-C_3N_4 sample: (**a**) survey, (**b**) C 1s, and (**c**) N 1s spectra.

To investigate the tribocatalytic activity of the g-C_3N_4 sample, N_2 fixation experiments were performed under stirring. Figure 5 depicts the tribocatalytic N_2 fixation performance with the different scavengers. When methanol is added as the positive charge scavenger, with the increase of the stirring time, the NH_4^+ content increases linearly [44]. The generation rate of NH_4^+ can reach 100.56 μmol·L^{-1}·g^{-1}·h^{-1} after 10 h stirring. It is 3.91 times higher than that without any scavengers. Since the methanol can consume the positive charges, the generation of the negative charges is promoted, which can enhance the tribocatalytic N_2 fixation performance effectively. It is worth noting that the reductive active radicals, such as the negative charges, are necessary in the N_2 fixation reaction [45]. TBA can react with hydroxyl radicals (OH) in solution as the radical scavenger [46,47]. Since the formation of ·OH requires the participation of positive charge (q^+) and hydroxide ion (OH^-), the addition of TBA promotes the consumption of q+ and effectively prolongs the lifetime of negative charge (q^-). Therefore, the addition of TBA is beneficial to the tribocatalytic nitrogen fixation of g-C_3N_4. Consequently, $KBrO_3$ as the negative charge scavenger is used to investigate the important role of the negative charges in this catalytic process [48]. It can be observed that the NH_4^+ generation rate is about 0.26 μmol·L^{-1}·g^{-1}·h^{-1}. It can be concluded that the addition of $KBrO_3$ is not beneficial for the N_2 fixation reaction, which accords with the theoretic expectation.

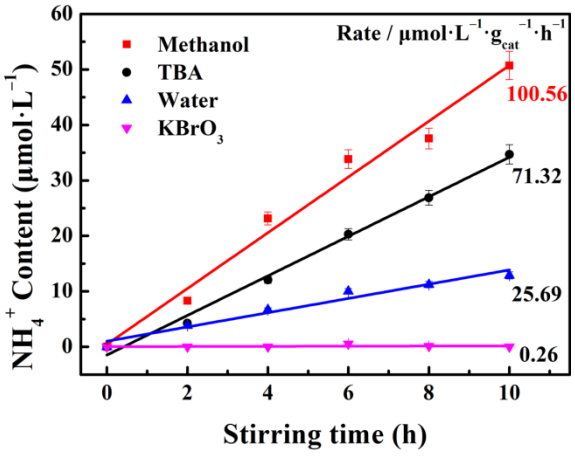

Figure 5. Tribocatalytic N_2 fixation performance of g-C_3N_4 with the different scavengers.

To further investigate the schematic mechanism of the tribocatalytic N_2 fixation reaction, the control experiments under the different addition have been performed as shown in Figure 6. There is scarcely any generation of NH_4^+ without a catalyst, which indicates that the addition of a catalyst is essential for the tribocatalytic N_2 fixation reaction. Additionally, the tribocatalytic performance associates with the contact area between the g-C_3N_4 catalyst and the stirring rod [49]. Therefore, control experiments with the different stirring rods were carried out. Rod I is the commercial PTFE-sealed rod. Two polyvinyl chloride (PVC) electrical tape rings with a width of 1mm were wound on the stirring rod to avoid contact between the catalyst and stirring rod as far as possible, and the stirring rod is named rod II. Obviously, with the decrease of the contact area, the NH_4^+ generation rate reduces gradually, indicating that the contact area is an important influencing factor of the tribocatalytic performance.

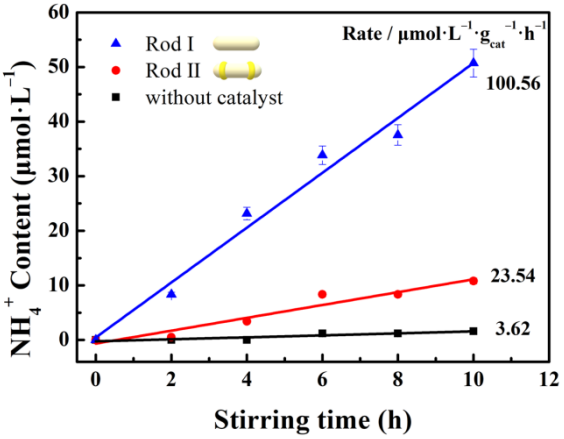

Figure 6. Tribocatalytic N_2 fixation performance of g-C_3N_4 with the different kinds of rods or without catalyst.

The influence of the stirring speed on the tribocatalytic performance was also considered. The much faster stirring speed provides much more contact times per minute, that is to say, the contact area is also enlarged relatively per minute. Consequently, the tribocatalytic performance would be enhanced. As depicted in Figure 7, the NH_4^+ generation rate is improved significantly from 15.63 to 100.56 μmol·L^{-1}·g^{-1}·h^{-1} with the stirring speed increasing from 400 to 1000 rpm, and a linear relationship between g-C_3N_4 tribocatalytic nitrogen fixation rate and stirring speed is observed. As the stirring speed increases, the friction frequency increases, and more active substances can be produced to participate in the nitrogen fixation process, so an efficient nitrogen fixation can be obtained.

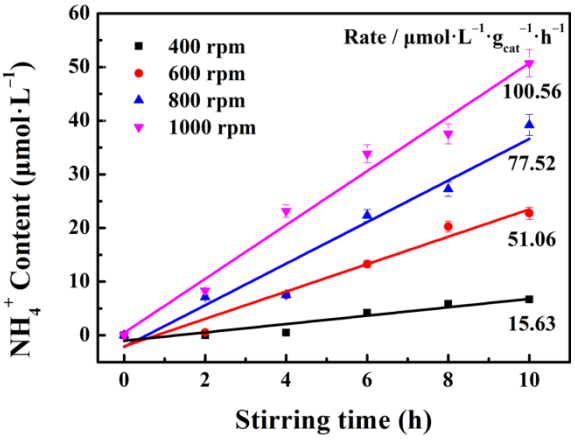

Figure 7. Tribocatalytic N_2 fixation performance of g-C_3N_4 under the different stirring speed.

The effect of contact area on the performance of g-C_3N_4 tribocatalytic N_2 fixation is investigated through adjusting the number of stirring rods. Figure 8 shows the nitrogen fixation effect with a different number of stirring rods. Obviously, the total contact area is strongly enlarged as the number of the stirring rods increases. As expected, the NH_4^+ generation rate is about 244.02 μmol·L^{-1}·g^{-1}·h^{-1} using three stirring rods, which is 2.43 times that of only one stirring rod. Typically, the contact area is usually proportional to the number of rods, but the NH_4^+ generation rate is not. For instance, the distribution of the catalyst is not uniform in suspension, which leads to inadequate contact between the rods and catalyst, that is to say, each stirring time may not necessarily induce the tribocatalytic reaction. Perhaps there are other influencing factors which influence the tribocatalytic performance. Consequently, the NH_4^+ generation rate is not in linear correlation with the number of stirring rods.

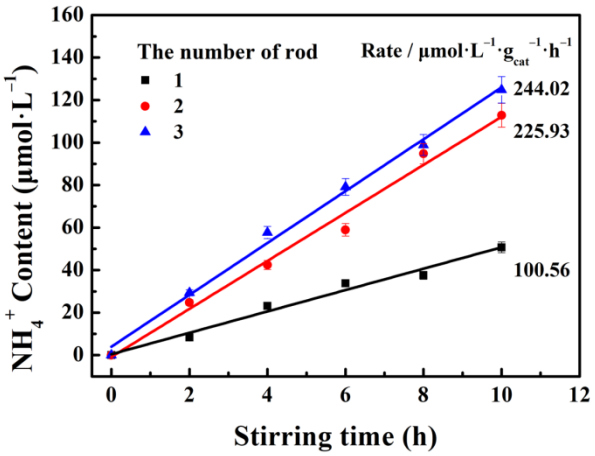

Figure 8. Tribocatalytic N_2 fixation performance of g-C_3N_4 with the different number of stirring rods.

Furthermore, the tribocatalytic nitrogen fixation performance of g-C_3N_4 was evaluated through comparison with other existing nitrogen fixation research. It can be seen from Table 1 that g-C_3N_4 can realize nitrogen fixation through both photocatalysis and tribocatalysis, and it has an excellent performance [50]. In addition, due to its large specific surface area, g-C_3N_4 has superior nitrogen fixation activity compared to other materials [51–55].

Table 1. Summary of ammonia fixation performance of different catalysts and different catalytic methods.

Catalysts	Ammonia Generation Rate/μmol·L^{-1}·g^{-1}·h^{-1}	Nitrogen Source	Scavenger	Catalytic Method
g-C_3N_4	100.56	air	methanol	Tribocatalysis [this work]
g-C_3N_4	160	air	methanol	Photocatalysis [50]
P25	52	N_2	water	Photocatalysis [51]
BiOCl	68.9	N_2	methanol	Photocatalysis [52]
FeS_2/CeO_2	90	N_2	water	Photocatalysis [53]
$KTa_{0.5}Nb_{0.5}O_3$	13.2	air	methanol	Piezocatalysis [54]
Ag/Bi_5O_7I	65.4	air	water	Piezocatalysis [55]

According to the previous analysis, the tribocatalytic mechanism of g-C_3N_4 is drawn in Figure 9. The friction between the g-C_3N_4 catalyst and the stirring rod is realized via mechanical stirring, which is accompanied by charge transfer. It is known from the empirical rule of triboelectrification, the g-C_3N_4 catalyst is more likely to lose electrons with positive charge than the stirring rod. Therefore, in the process of tribocatalysis, the

stirring rod is negatively charged and the catalyst is positively charged. The above process can be represented by Equation (1) [56]:

$$g - C_3N_4 + \text{stirring rod} \xrightarrow{\text{Friction}} g - C_3N_4(q^+) + \text{stirring rod}(q^-) \quad (1)$$

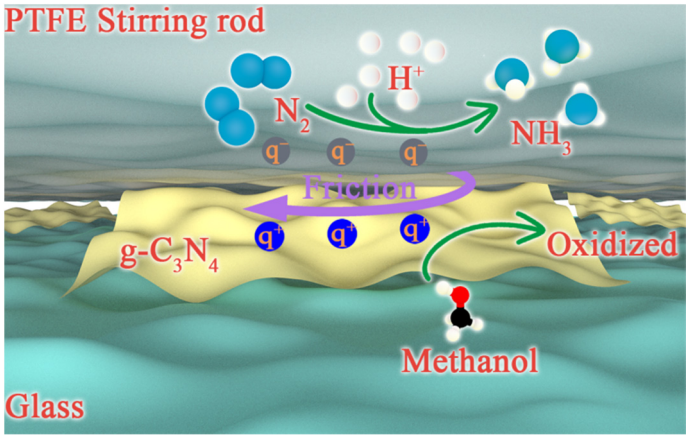

Figure 9. The schematic diagram for the tribocatalytic mechanism of g-C_3N_4.

Then methanol as the positive charge scavenger will react with q+ to avoid NH_4^+ being oxidized [37]. In addition, q^- will react with N_2 to produce NH_4^+, which is dissolved in DI water to form NH_4^+. The main reaction process is described in Equations (2)–(4) [57,58]:

$$q^+ + CH_3OH \rightarrow CH_3OH^+ \quad (2)$$

$$6\,q^- + N_2 + 6H^+ \rightarrow 2NH_3 \quad (3)$$

$$NH_3 + H_2O \rightarrow NH_3{\cdot}H_2O \rightleftharpoons NH_4^+ + OH^- \quad (4)$$

In this work, g-C_3N_4 exhibits excellent tribocatalytic performance in the N_2 fixation process. Though, as a matter of fact, the applications of the tribocatalysis are not restricted in this field. In the past few years, He et al. have achieved excellent tribocatalytic performance on removal of the heavy metal ion Cr^{6+} through using commercial iron turning with amorphous iron oxides. After 36 h stirring, the removal ratio of Cr^{6+} can reach about 98% [59]. Additionally, Li et al. have successfully produced flammable gases such as CO, CH_4 and H_2 through harvesting mechanical energy with TiO_2 nanoparticles [20]. In the future, g-C_3N_4 has potential applications in wastewater treatment and energy generation fields via tribocatalysis.

4. Conclusions

In summary, g-C_3N_4 has been fabricated successfully via the chemical blowing method and shows excellent tribocatalytic performance in the reduction of nitrogen to NH_4^+. After 10 h of continuous stirring at 1000 rpm in the dark, the generation rate of NH_4^+ can reach 100.56 $\mu mol{\cdot}L^{-1}{\cdot}g^{-1}{\cdot}h^{-1}$ using methanol as a positive charges scavenger, which is 3.91 times higher than that without any scavengers. Furthermore, the performance of the tribocatalytic nitrogen fixation of g-C_3N_4 can be effectively optimized through increasing the stirring speed or number of stirring rods. Consequently, g-C_3N_4 has the remarkable potential application in the tribocatalytic N_2 fixation reaction. Tribocatalysis has a bright application prospect in energy development fields such as nitrogen fixation, carbon dioxide reduction and water decomposition in the future.

Author Contributions: Conceptualization, J.G., T.X. and Z.W.; methodology, J.G., L.R. and X.D.; software, J.G.; validation, J.G. and L.R.; formal analysis, Z.W.; investigation, J.G. and L.R.; resources, H.L. and S.H.; data curation, J.G.; writing—original draft preparation, J.G. and L.R.; writing—review and editing, Z.W.; visualization, Z.W. and Y.J.; supervision, Z.W.; project administration, Z.W.

and Y.J.; funding acquisition, Z.W. All authors have read and agreed to the published version of the manuscript.

Funding: This research was funded by the National Natural Science Foundation of China (grant numbers 51872264, 22179108); Key Research and Development Projects of Shaanxi Province (grant number 2020GXLH-Z-032); Shaanxi Provincial Natural Science Foundation of China (grant number 2020JM-579); Hebei Key Laboratory of Dielectric and Electrolyte Functional Material, Northeastern University at Qinhuangdao (No. HKDEFM2021101); Doctoral Research Start-up Fund project of Xi'an Polytechnic University (Grant Number: 107020589); Shaanxi Provincial High-Level Talents Introduction Project (Youth Talent Fund); Key Research and Development Program of Zhejiang Province (2021C01006).

Data Availability Statement: The data presented in this study are available in this article.

Conflicts of Interest: The authors declare no conflict of interest.

References

1. Chen, M.; Jia, Y.; Li, H.; Wu, Z.; Huang, T.; Zhang, H. Enhanced pyrocatalysis of the pyroelectric $BiFeO_3$/g-C_3N_4 heterostructure for dye decomposition driven by cold-hot temperature alternation. *J. Adv. Ceram.* **2021**, *10*, 338–346. [CrossRef]
2. Iwamoto, M.; Akiyama, M.; Aihara, K.; Deguchi, T. Ammonia synthesis on wool-like Au, Pt, Pd, Ag, or Cu electrode catalysts in nonthermal atmospheric-pressure plasma of N_2 and H_2. *ACS Catal.* **2017**, *7*, 6924–6929. [CrossRef]
3. Singh, A.R.; Rohr, B.A.; Schwalbe, J.A.; Cargnello, M.; Chan, K.; Jaramillo, T.F.; Chorkendorff, I.; Nørskov, J.K. Electrochemical Ammonia synthesis—The selectivity challenge. *ACS Catal.* **2017**, *7*, 706–709. [CrossRef]
4. Vojvodic, A.; Medford, A.J.; Studt, F.; Abild Pedersen, F.; Khan, T.S.; Bligaard, T.; Nørskov, J.K. Exploring the limits: A low-pressure, low-temperature haber–bosch process. *Chem. Phys. Lett.* **2014**, *598*, 108–112. [CrossRef]
5. Sadeghzadeh-Attar, A. Photocatalytic degradation evaluation of N-Fe co-doped aligned TiO_2 nanorods based on the effect of annealing temperature. *J. Adv. Ceram.* **2020**, *9*, 107–122. [CrossRef]
6. Chen, X.; Li, N.; Kong, Z.; Ong, W.J.; Zhao, X. Photocatalytic fixation of nitrogen to ammonia: State-of-the-art advancements and future prospects. *Mater. Horiz.* **2018**, *5*, 9–27. [CrossRef]
7. Luo, Y.; Pu, T.; Fan, S.; Liu, H.; Zhu, J. Enhanced piezoelectric properties in low-temperature sintering PZN-PZT ceramics by adjusting Zr/Ti ratio. *J. Adv. Dielect.* **2022**, *12*, 2250001. [CrossRef]
8. Wang, Q.; Guo, J.; Chen, P. Recent progress towards mild-condition ammonia synthesis. *J. Energy Chem.* **2019**, *36*, 25–36. [CrossRef]
9. Xu, X.; Xiao, L.; Wu, Z.; Jia, Y.; Ye, X.; Wang, F.; Yuan, B.; Yu, Y.; Huang, H.; Zou, G. Harvesting vibration energy to piezo-catalytically generate hydrogen through Bi_2WO_6 layered-perovskite. *Nano Energy* **2020**, *78*, 105351. [CrossRef]
10. Panda, P.K.; Sahoo, B.; Sureshkumar, V.; Politova, E.D. Effect of Zr^{4+} on piezoelectric, dielectric and ferroelectric properties of barium calcium titanate lead-free ceramics. *J. Adv. Dielect.* **2021**, *11*, 2150024. [CrossRef]
11. Kajdas, C.; Hiratsuka, K. Tribochemistry, tribocatalysis, and the negative-ion-radical action mechanism. *Proc. IMechE Part J J. Eng. Tribol.* **2009**, *223*, 827–848. [CrossRef]
12. Fan, F.R.; Tang, W.; Wang, Z.L. Flexible nanogenerators for energy harvesting and self-powered electronics. *Adv. Mater.* **2016**, *28*, 4283–4305. [CrossRef] [PubMed]
13. Fan, F.R.; Xie, S.; Wang, G.W.; Tian, Z.Q. Tribocatalysis: Challenges and perspectives. *Sci. China Chem.* **2021**, *64*, 1609–1613. [CrossRef]
14. Wang, Z.L. Triboelectric nanogenerators as new energy technology for self-powered systems and as active mechanical and chemical sensors. *ACS Nano* **2013**, *7*, 9533–9557. [CrossRef]
15. Shaw, P.E.; Barton, E.H. Experiments on tribo-electricity. I.—The tribo-electric series. *Proc. R. Soc. Lond. A* **1917**, *94*, 16–33.
16. Chen, C.; Wang, Y.; Li, J.; Wu, C.; Yang, G. Piezoelectric, ferroelectric and pyroelectric properties of (100 − x) Pb ($Mg_{1/3}Nb_{2/3}$) O_3 − x$PbTiO_3$ ceramics. *J. Adv. Dielect.* **2022**, 2250002. [CrossRef]
17. Wu, M.; Lei, H.; Chen, J.; Dong, X. Friction energy harvesting on bismuth tungstate catalyst for tribocatalytic degradation of organic pollutants. *J. Colloid Interface Sci.* **2021**, *587*, 883–890. [CrossRef] [PubMed]
18. Hu, J.; Ma, W.; Pan, Y.; Chen, Z.; Zhang, Z.; Wan, C.; Sun, Y.; Qiu, C. Resolving the tribo-catalytic reaction mechanism for biochar regulated zinc oxide and its application in protein transformation. *J. Colloid Interface Sci.* **2022**, *607*, 1908–1918. [CrossRef] [PubMed]
19. Wang, C. Piezo-catalytic degradation of havriliak–negami type. *J. Adv. Dielect.* **2019**, *9*, 1950021. [CrossRef]
20. Li, P.; Tang, C.; Xiao, X.; Jia, Y.; Chen, W. Flammable gases produced by TiO_2 nanoparticles under magnetic stirring in water. *Friction* **2022**, *10*, 1127–1133. [CrossRef]
21. Yan, H.; Li, J.; Zhang, M.; Zhao, Y.; Feng, Y.; Zhang, Y. Enhanced corrosion resistance and adhesion of epoxy coating by two-dimensional graphite-like g-C_3N_4 nanosheets. *J. Colloid Interface Sci.* **2020**, *579*, 152–161. [CrossRef]
22. Mishra, A.; Mehta, A.; Basu, S.; Shetti, N.P.; Reddy, K.R.; Aminabhavi, T.M. Graphitic carbon nitride (g–C_3N_4)–based metal-free photocatalysts for water splitting: A review. *Carbon* **2019**, *149*, 693–721. [CrossRef]

23. Lei, H.; Wu, M.; Mo, F.; Ji, S.; Dong, X.; Jia, Y.; Wang, F.; Wu, Z. Efficiently harvesting the ultrasonic vibration energy of two-dimensional graphitic carbon nitride for piezocatalytic degradation of dichlorophenols. *Environ. Sci. Nano* **2021**, *8*, 1398–1407. [CrossRef]
24. Yang, W.; Chen, Y.; Gao, S.; Sang, L.; Tao, R.; Sun, C.; Shang, J.K.; Li, Q. Post-illumination activity of Bi_2WO_6 in the dark from the photocatalytic "memory" effect. *J. Adv. Ceram.* **2021**, *10*, 355–367. [CrossRef]
25. Mo, F.; Liu, Y.; Xu, Y.; He, Q.; Sun, P.; Dong, X. Photocatalytic elimination of moxifloxacin by two-dimensional graphitic carbon nitride nanosheets: Enhanced activity, degradation mechanism and potential practical application. *Sep. Purif. Technol.* **2022**, *292*, 121067. [CrossRef]
26. Yu, Z.; Mao, K.; Feng, Y. Single-source-precursor synthesis of porous W-containing SiC-based nanocomposites as hydrogen evolution reaction electrocatalysts. *J. Adv. Ceram.* **2021**, *10*, 1338–1349. [CrossRef]
27. Han, C.; Su, P.; Tan, B.; Ma, X.; Lv, H.; Huang, C.; Wang, P.; Tong, Z.; Li, G.; Huang, Y.; et al. Defective ultra-thin two-dimensional g-C_3N_4 photocatalyst for enhanced photocatalytic H_2 evolution activity. *J. Colloid Interface Sci.* **2021**, *581*, 159–166. [CrossRef]
28. Aggarwal, M.; Basu, S.; Shetti, N.P.; Nadagouda, M.N.; Kwon, E.E.; Park, Y.K.; Aminabhavi, T.M. Photocatalytic carbon dioxide reduction: Exploring the role of ultrathin 2D graphitic carbon nitride (g-C_3N_4). *Chem. Eng. J.* **2021**, *425*, 131402. [CrossRef]
29. Zhang, X.; Yuan, X.; Jiang, L.; Zhang, J.; Yu, H.; Wang, H.; Zeng, G. Powerful combination of 2D g-C_3N_4 and 2D nanomaterials for photocatalysis: Recent advances. *Chem. Eng. J.* **2020**, *390*, 124475. [CrossRef]
30. Sun, Z.; Wang, H.; Wu, Z.; Wang, L. g-C_3N_4 based composite photocatalysts for photocatalytic CO_2 reduction. *Catal. Today* **2018**, *300*, 160–172. [CrossRef]
31. Zhang, Y.; Di, J.; Ding, P.; Zhao, J.; Gu, K.; Chen, X.; Yan, C.; Yin, S.; Xia, J.; Li, H. Ultrathin g-C_3N_4 with enriched surface carbon vacancies enables highly efficient photocatalytic nitrogen fixation. *J. Colloid Interface Sci.* **2019**, *553*, 530–539. [CrossRef] [PubMed]
32. Vilé, G.; Di Liberto, G.; Tosoni, S.; Sivo, A.; Ruta, A.; Nachtegaal, M.; Clark, A.H.; Agnoli, S.; Zou, Y.; Savateev, A.; et al. Azide-alkyne click chemistry over a heterogeneous copper-based single-atom catalyst. *ACS Catal.* **2022**, *12*, 2947–2958. [CrossRef]
33. Liu, J.; Zou, Y.; Cruz, D.; Savateev, A.; Antonietti, M.; G, Vilé. Ligand–metal charge transfer induced via adjustment of textural properties controls the performance of single-atom catalysts during photocatalytic degradation. *ACS Appl. Mater. Interfaces* **2021**, *13*, 25858–25867. [CrossRef] [PubMed]
34. Yan, J.; Han, X.; Qian, J.; Liu, J.; Dong, X.; Xi, F. Preparation of 2D graphitic carbon nitride nanosheets by a green exfoliation approach and the enhanced photocatalytic performance. *J. Mater. Sci.* **2017**, *52*, 13091–13102. [CrossRef]
35. Yang, Z.; Li, J.; Cheng, F.; Chen, Z.; Dong, X. BiOBr/protonated graphitic C_3N_4 heterojunctions: Intimate interfaces by electrostatic interaction and enhanced photocatalytic activity. *J. Alloys Compd.* **2015**, *634*, 215–222. [CrossRef]
36. Zhao, Y.; Shi, R.; Bian, X.; Zhou, C.; Zhao, Y.; Zhang, S.; Wu, F.; Waterhouse, G.I.N.; Wu, L.Z.; Tung, C.H.; et al. Ammonia detection methods in photocatalytic and electrocatalytic experiments: How to improve the reliability of NH_3 production rates? *Adv. Sci.* **2019**, *6*, 1802109. [CrossRef] [PubMed]
37. Shi, A.; Li, H.; Yin, S.; Hou, Z.; Rong, J.; Zhang, J.; Wang, Y. Photocatalytic NH_3 versus H_2 evolution over g-C_3N_4/CsxWO$_3$: O_2 and methanol tipping the scale. *Appl. Catal. B Environ.* **2018**, *235*, 197–206. [CrossRef]
38. Yao, C.; Yuan, A.; Wang, Z.; Lei, H.; Zhang, L.; Guo, L.; Dong, X. Amphiphilic two-dimensional graphitic carbon nitride nanosheets for visible-light-driven phase-boundary photocatalysis. *J. Mater. Chem. A* **2019**, *7*, 13071–13079. [CrossRef]
39. Tian, N.; Huang, H.; He, Y.; Guo, Y.; Zhang, T.; Zhang, Y. Mediator-free direct Z-scheme photocatalytic system: $BiVO_4$/g-C_3N_4 organic–inorganic hybrid photocatalyst with highly efficient visible-light-induced photocatalytic activity. *Dalton Trans.* **2015**, *44*, 4297–4307. [CrossRef]
40. Ma, T.Y.; Tang, Y.; Dai, S.; Qiao, S.Z. Proton-functionalized two-dimensional graphitic carbon nitride nanosheet: An excellent metal-/label-free biosensing platform. *Small* **2014**, *10*, 2382–2389. [CrossRef]
41. Yan, H.; Yang, H. TiO_2–g-C_3N_4 composite materials for photocatalytic H_2 evolution under visible light irradiation. *J. Alloys Compd.* **2011**, *509*, L26–L29. [CrossRef]
42. Zhu, B.; Xia, P.; Ho, W.; Yu, J. Isoelectric point and adsorption activity of porous g-C_3N_4. *Appl. Surf. Sci.* **2015**, *344*, 188–195. [CrossRef]
43. Ye, L.; Liu, J.; Jiang, Z.; Peng, T.; Zan, L. Facets coupling of BiOBr-g-C_3N_4 composite photocatalyst for enhanced visible-light-driven photocatalytic activity. *Appl. Catal. B Environ.* **2013**, *142–143*, 1–7. [CrossRef]
44. Wei, Y.; Cheng, G.; Xiong, J.; Zhu, J.; Gan, Y.; Zhang, M.; Li, Z.; Dou, S. Synergistic impact of cocatalysts and hole scavenger for promoted photocatalytic H2 evolution in mesoporous TiO_2-NiS_x hybrid. *J. Energy Chem.* **2019**, *32*, 45–56. [CrossRef]
45. Kitano, M.; Kanbara, S.; Inoue, Y.; Kuganathan, N.; Sushko, P.V.; Yokoyama, T.; Hara, M.; Hosono, H. Electride support boosts nitrogen dissociation over ruthenium catalyst and shifts the bottleneck in ammonia synthesis. *Nat. Commun.* **2015**, *6*, 6731. [CrossRef] [PubMed]
46. Pei, C.; Tan, J.; Li, Y.; Yao, G.; Jia, Y.; Ren, Z.; Liu, P.; Zhang, H. Effect of Sb-site nonstoichiometry on the structure and microwave dielectric properties of $Li_3Mg_2Sb_{1-x}O_6$ ceramics. *J. Adv. Ceram.* **2020**, *9*, 588–594. [CrossRef]
47. Ruan, L.; Jia, Y.; Guan, J.; Xue, B.; Huang, S.; Wu, Z.; Li, G.; Cui, X. Highly piezocatalysis of metal-organic frameworks material ZIF-8 under vibration. *Sep. Purif. Technol.* **2022**, *283*, 120159. [CrossRef]
48. Zhang, B.; Sun, R.; Wang, F.; Feng, T.; Zhang, P.; Luo, H. Pyroelectric properties of 91.5 $Na_{0.5}Bi_{0.5}TiO_3$-8.5 $K_{0.5}Bi_{0.5}TiO_3$ lead-free single crystal. *J. Adv. Dielect.* **2021**, *11*, 2150023. [CrossRef]

49. Zhao, J.; Chen, L.; Luo, W.; Li, H.; Wu, Z.; Xu, Z.; Zhang, Y.; Zhang, H.; Yuan, G.; Gao, J.; et al. Strong tribo-catalysis of zinc oxide nanorods via triboelectrically-harvesting friction energy. *Ceram. Int.* **2020**, *46*, 25293–25298. [CrossRef]
50. Dong, G.; Ho, W.; Wang, C. Selective photocatalytic N_2 fixation dependent on g-C_3N_4 induced by nitrogen vacancies. *J. Mater. Chem. A.* **2015**, *3*, 23435–23441. [CrossRef]
51. Liao, Y.; Lin, J.; Cui, B.; Xie, G.; Hu, S. Well-dispersed ultrasmall ruthenium on TiO_2 (P25) for effective photocatalytic N_2 fixation in ambient condition. *J. Photochem. Photobiol. A Chem.* **2020**, *387*, 112100. [CrossRef]
52. Li, H.; Shang, J.; Shi, J.; Zhao, K.; Zhang, L. Facet-dependent solar ammonia synthesis of BiOCl nanosheets via a proton-assisted electron transfer pathway. *Nanoscale* **2016**, *8*, 1986–1993. [CrossRef] [PubMed]
53. Sultana, S.; Mansingh, S.; Parida, K.M. Phosphide protected FeS_2 anchored oxygen defect oriented CeO_2NS based ternary hybrid for electrocatalytic and photocatalytic N_2 reduction to NH_3. *J. Mater. Chem. A* **2019**, *7*, 9145–9153. [CrossRef]
54. Chen, L.; Wang, J.; Li, X.; Zhang, J.; Zhao, C.; Hu, X.; Lin, H.; Zhao, L.; Wu, Y.; He, Y. Facile preparation of $Ag_2S/KTa_{0.5}Nb_{0.5}O_3$ heterojunction for enhanced performance in catalytic nitrogen fixation via photocatalysis and piezo-photocatalysis. *Green Energy Environ.* 2022, *in press*. [CrossRef]
55. Chen, L.; Zhang, W.; Wang, J.; Li, X.; Li, Y.; Hu, X.; Zhao, L.; Wu, Y.; He, Y. High piezo/photocatalytic efficiency of Ag/Bi_5O_7I nanocomposite using mechanical and solar energy for N_2 fixation and methyl orange degradation. *Green Energy Environ.* 2021; *in press*. [CrossRef]
56. Li, P.; Wu, J.; Wu, Z.; Jia, Y.; Ma, J.; Chen, W.; Zhang, L.; Yang, J.; Liu, Y. Strong tribocatalytic dye decomposition through utilizing triboelectric energy of barium strontium titanate nanoparticles. *Nano Energy* **2019**, *63*, 103832. [CrossRef]
57. Jung, B.; Abu-Rub, F.; El-Ghenymy, A.; Deng, W.; Li, Y.; Batchelor, B.; Abdel-Wahab, A. Photocatalytic reduction of chlorate in aqueous TiO_2 suspension with hole scavenger under simulated solar light. *Emerg. Mater.* **2021**, *4*, 435–446. [CrossRef]
58. Diarmand-Khalilabad, H.; Habibi-Yangjeh, A.; Seifzadeh, D.; Asadzadeh-Khaneghah, S.; Vesali-Kermani, E. g-C_3N_4 nanosheets decorated with carbon dots and CdS nanoparticles: Novel nanocomposites with excellent nitrogen photofixation ability under simulated solar irradiation. *Ceram. Int.* **2019**, *45*, 2542–2555. [CrossRef]
59. He, J.; Zhai, W.; Wang, S.; Wang, Y.; Li, W.; He, G.; Hou, X.; Liu, J.; He, Q. Persistently high Cr^{6+} removal rate of centi-sized iron turning owing to tribocatalysis. *Mater. Today Phys.* **2021**, *19*, 100408. [CrossRef]